applied sciences

MDPI

Article

Experimental Study on Creep Characteristics of Unloaded Rock Masses for Excavation of Rock Slopes in Cold Areas

Xingzhou Chen *, Hai Jiang, Lili Chen, Wei Du and Sheng Gong

School of Architecture and Civil Engineering, Xi'an University of Science and Technology, Xi'an 710054, China
* Correspondence: xzchen0416@163.com

Abstract: Seasonal freeze–thaw environments are one of the key factors that aggravate the mechanical strength decay of excavated and unloaded rock masses on reservoir banks in cold areas. To study the time-dependent mechanical properties of an excavated and unloaded rock mass on a bank slope under freeze–thaw action, triaxial unloading tests were carried out on sandstone, freeze–thaw tests simulating freezing strength were conducted, and triaxial creep tests were implemented with graded incremental loading on unloaded specimens subjected to freeze–thaw action. The test results showed that the total deformation of the unloaded specimens is significantly increased compared with the conventional specimens, and the lateral direction is more likely to produce creep behaviour than the axial direction. The level of confining pressure determines the level of creep deformation of unloaded specimens and affects the variation law of creep rate. The creep behaviour of the unloaded specimens is aggravated by freeze–thaw action and, the longer the freezing period, the larger the creep strain share, and the creep rate increases significantly. The creep damage pattern of the unloaded specimens subjected to freeze–thaw action is mainly manifested as shear damage, and the creep process intensifies the derivation of tension-type cracks in the specimens. The higher the confining pressure of the unloaded specimen, the more obvious the plastic characteristics and the weaker the brittle characteristics during creep failure. The freeze–thaw action significantly reduces the long-term strength of the unloaded specimen, which is approximately 50~55% of the instantaneous strength. The long-term strength decays significantly with an increasing freezing period, and the research results can provide a theoretical reference for the evaluation of the long-term stability of excavated and unloaded rock masses in cold areas.

Keywords: cold region slopes; unloaded rock mass; unloading test; freeze–thaw action; creep properties

Citation: Chen, X.; Jiang, H.; Chen, L.; Du, W.; Gong, S. Experimental Study on Creep Characteristics of Unloaded Rock Masses for Excavation of Rock Slopes in Cold Areas. *Appl. Sci.* **2023**, *13*, 3138. https://doi.org/10.3390/app13053138

Academic Editors: Chunlai Wang, Shaojie Chen, Weijian Yu, Guangjin Wang and Xiaoshuang Li

Received: 17 January 2023
Revised: 24 February 2023
Accepted: 24 February 2023
Published: 28 February 2023

1. Introduction

Engineering practice has shown that the strength characteristics of a rock body disturbed by excavation and unloading have obvious time effects [1,2] and, if appropriate support is not carried out in time after excavation, local instability or overall instability may occur with the development of time, which may lead to collapse damage and other engineering accidents, such as Frank slide [3] and Okayama slide [4].

In recent decades, the problem of creep mechanics of rocks has been widely studied by many scholars; the research is mainly focused on creep deformation characteristics [5,6], macroscopic and detailed damage patterns [7,8], long-term strength [9,10], and so on. The essence of excavation for rock is an unloading process and the deformation of the rock after excavation and unloading also has a time effect [11]. The rock exhibits significantly different mechanical properties under unloading conditions than under loading conditions [12]. As Huang [13] performed unloading creep tests on soft rock, and found that the variation in the change in the confining pressure value under unloading conditions is the main cause of creep deformation and lateral expansion of soft rock; Zhu [14] performed unloading creep tests on marble at different initial axial stress levels and found that the long-term strength of rock samples under unloading conditions was significantly less than under

triaxial compression. Zvonko [15] proposed a creep model for the excavation unloading behavior of rock that can describe the deformation of the rock with time after being unloaded. Currently, most of the studies have simulated the excavation unloading process by applying an unloading stress path to the original rock samples, and the damaged rock mass after excavation unloading is rarely considered as the object of study. The differential characteristics of the unloaded damaged rock samples and the original rock samples can be found in [16].

In addition, with the further shift of China's engineering construction to the northwest, the environmental problem of seasonal freezing and thawing in the site area has become more and more prominent, which seriously affects the stability of the excavation slope. Rock material is a three-phase material consisting of solid particles, water, and air. When the temperature is too low, the water stored in the pores of the rock is converted from the liquid phase to the solid phase, and the volume expands by about 9% [17,18], which exerts a frost swelling force on the surrounding rock, thus accelerating the deterioration of the rock structure and making the excavation slope more dangerous. Maxim [19] summarized the main factors affecting freeze–thaw damage in rocks, including the pore structure characteristics, effective water content, cooling rate, freezing period, and minimum temperature of the rock. Jihwan [20] studied the changes in the internal fine structure of rocks during freezing and thawing using CT scanning and electron microscopy, and found that water in the pores of rocks undergoes a water–ice phase change under low temperature conditions, causing rock particles to fall off, fractures to increase, and porosity to increase, which leads to lower longitudinal wave velocity, lower quality, and lower strength of rocks. They also compared the test results of different types of rocks and found that the magnitude of initial porosity is an important factor affecting the degree of rock deterioration. Some scholars have studied the effect of freeze–thaw action on the creep mechanical properties of rocks. Chen [21] studied the mechanical characteristics of freeze–thaw on quartzite under short-term and long-term loading, and found that freeze–thaw had a small effect on the mechanical properties of sandstone under short-term loading, but had a significant effect on the time-dependent mechanical characteristics of sandstone under long-term loading. Li [22] described the creep behavior of rocks under freeze–thaw action and long-term loading by establishing a nonlinear creep damage equation.

Synthesizing the available research results, abundant results have been obtained on unloading creep and freeze–thaw creep of rocks, and the theoretical system is well established. However, the long-term mechanical properties of rock masses subjected to freeze–thaw action after excavation and unloading in cold regions are less studied. In fact, after the excavation of the high and steep slope is completed, the rocks originally stored underground are exposed to the superficial layer of the ground and are again highly susceptible to further erosion because of the low temperature environment. Therefore, in this paper, we decided to study the long-term mechanical properties of the rock under the conditions of both excavation unloading and freeze–thaw action, in order to provide a reference for the safety and long-term stability evaluation of excavated slopes in cold regions.

2. Materials and Methods

2.1. Unloaded Sample Preparation

Sandstone samples were prepared in standard cylinders [23], 100 mm in height and 50 mm in diameter. The rock samples with similar properties were selected by the method of longitudinal wave velocity measurement. The average quality of the selected rock sample is 419.64 g, density is 2.15 g·cm^{-3}, longitudinal wave velocity is 2294 m·s^{-1}, porosity is 14.95%, and uniaxial strength is 62.8 MPa. The sandstone samples and triaxial test equipment are shown in Figure 1.

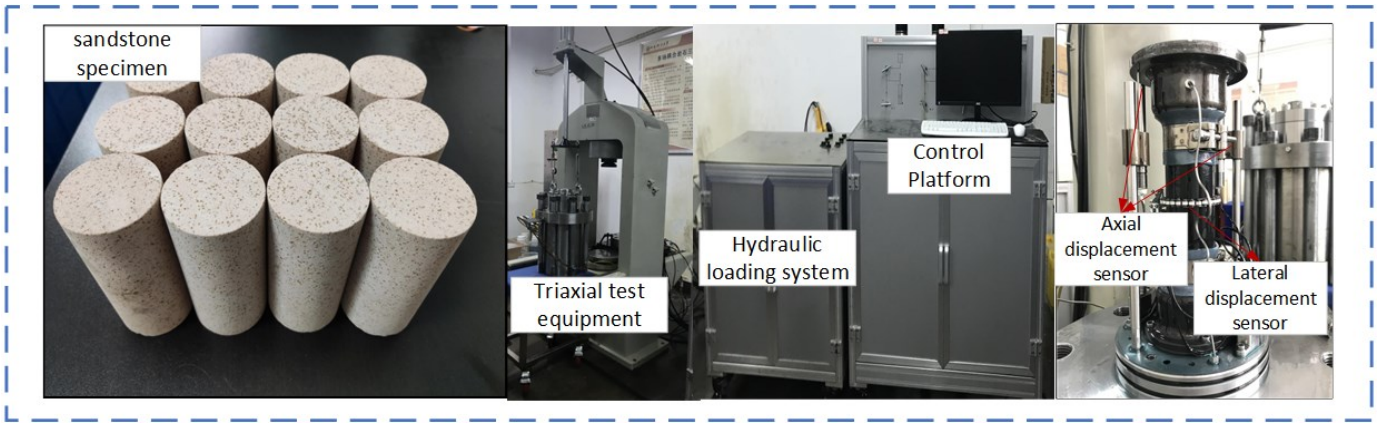

Figure 1. Sandstone specimens and triaxial test equipment (where (**c**) shows the displacement sensors, consisting of two axial displacement sensors parallel to the height direction of the specimen and a chain displacement sensor around the middle of the specimen. When the specimen is compressed, the axial displacement sensor is compressed at the same time, and the lateral displacement sensor is elongated with the lateral expansion of the sample, with the height of the sample being compressed and the size of the radial expansion able to be measured to obtain the axial and lateral strains. The measuring accuracy is 0.001 mm). (**a**) Sandstone specimens; (**b**) triaxial test equipment; (**c**) displacement sensors.

In the process of engineering slope excavation, there are different excavation levels and different excavation rates for the rock mass within different areas. In this paper, the values of the confining pressure of sandstone specimens at the time of unloading damage were determined by pretesting the common sandstone samples for unloading confining pressure damage. After comparing the changes in the stress–strain curve in the unloading test and the morphological characteristics of the sample, 75% of the confining pressure unloading (i.e., 75% of the confining pressure value from the beginning of unloading under the corresponding confining pressure to the confining pressure value at the time of unloading damage) was finally selected as the change in confining pressure in this unloading test. The formula for the value of confining pressure unloading is as follows:

$$\Delta\sigma_3 = \left(\frac{\sigma_3 - \sigma_3^i}{\sigma_3 - \sigma_d}\right) \times 100\% \quad (1)$$

where σ_3^i is the confining pressure at the end of the unloading, σ_3 is the initial design confining pressure, and σ_d is the final confining pressure when the sample is damaged.

The stress paths taken in this unloading test are presented in Figure 2 and the loading or unloading rates for each phase are labelled. Step I: The rock sample has specific pore structure characteristics under the original ground stress environment when it was not mined, the stress state of the rock sample changed after mining, and the structural characteristics changed accordingly. Therefore, when preparing unloaded damaged rock samples, we first simulate the initial stress state of the rock sample by loading the hydrostatic pressure ($\sigma_1 = \sigma_3$), as well as not destroying the pore structure characteristics, as in section *oa* in Figure 2. Step II: Keeping the confining pressure σ_3 constant, continue to load the axial pressure σ_1 to 75% of the peak triaxial strength, corresponding to the confining pressure value, as in section *ab* in Figure 2. Step III: Simulate the excavation disturbance process by the method of unloading the confining pressure, keep the axial pressure σ_1 unchanged, and unload the confining pressure σ_3 to the set value, as in section *bc* in Figure 2. Step IV: Unload the axial pressure to the set value (end of this stage, $\sigma_1 = \sigma_3$), as in section *cd* in Figure 2. Step V: Unload the hydrostatic pressure stage, as in the section *do* in Figure 2.

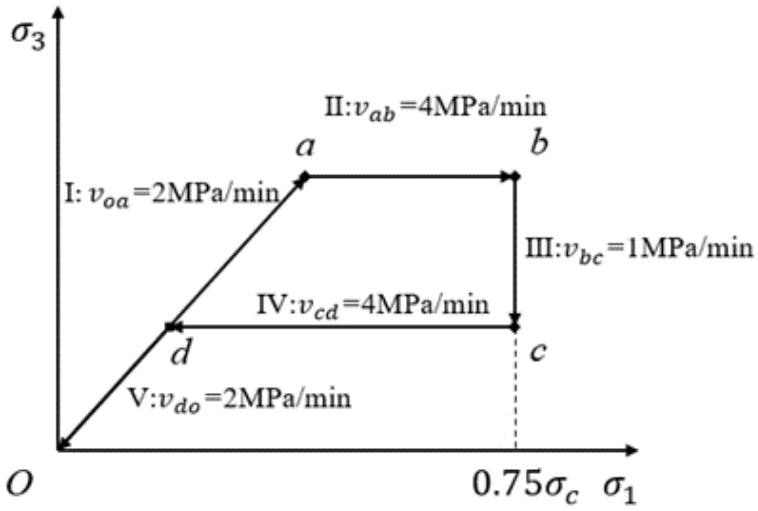

Figure 2. Unloading test stress path (σ_c indicates peak triaxial strength).

Two initial confining pressure values were set in this test: 15 MPa and 21 MPa. Two points need to be clarified. Firstly, the initial confining pressure value here refers to the stress state of the rock before the slope excavation, and the confining pressure value after unloaded is used in the subsequent creep experiments. Secondly, the higher confining value of the confining pressure is chosen to obtain a significant unloading effect.

Triaxial loading and triaxial unloading tests were conducted on saturated sandstone. At an initial confining pressure of 15 MPa, the triaxial peak strength of the sandstone was 160.8 MPa, the unloading damage confining pressure value was 4 MPa, and the residual confining pressure value of the unloaded specimen was 6.75 MPa. At an initial confining pressure of 21 MPa, the triaxial peak strength was 201 MPa, the unloading damage confining pressure value was 9 MPa, and the residual confining pressure value of the unloaded specimen was 12 MPa.

Figure 3 shows the stress–strain curve of the unloading test. As seen in the figure, the unloading stress–strain curve can be divided into the axial pressure loading phase with approximate linear elastic growth, the unloading confining pressure phase with significant lateral expansion, and the unloading sampling phase with deformation recovery. Axial pressure loading stage (A→B): with the increase in axial stress, the stress–strain curve 27 February 2023 exhibits an approximately linear growth trend; this stage is mainly dominated by the elastic deformation of the pore skeleton contraction, and axial compression deformation dominates. Unloading confining pressure stage (B→C): the confining pressure decreases, the deviating stress continues to increase, the lateral expansion caused by the weakening of lateral restraint continues to increase, the primary fracture expansion and the new fracture derivation are the main reasons for the unloading damage of the specimen, the axial strain is small at this stage, and the lateral expansion deformation dominates. Unloading sampling stage (C→D): This stage unloads according to the original loading path. The deformation of the specimen is recovered during the unloading process, but not entirely, and there is some unrecoverable plastic damage, mainly lateral damage deformation. Axial damage deformation is small. Comparing the unloading stress–strain curves under the two confining pressure conditions, it can be seen that there is a greater deviating stress under the high confining pressure conditions, and the unloading response is more obvious, specifically in terms of greater strain variation and more unrecoverable plastic damage deformation.

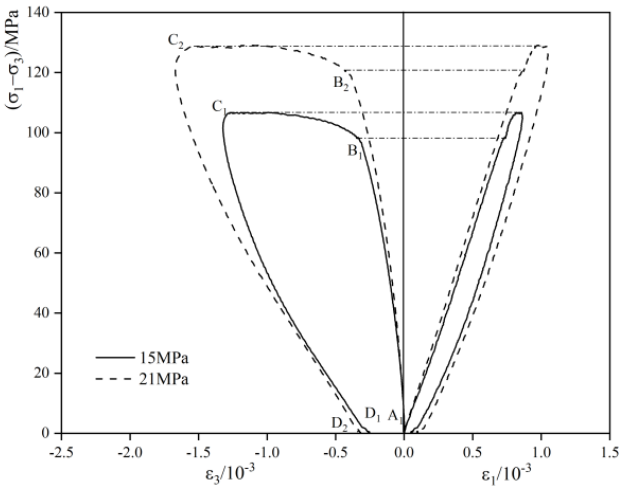

Figure 3. Unloading stress−strain curve.

2.2. Freeze–Thaw Environment Simulation Test

The test was conducted after saturating the unloaded samples prepared in Section 2.1 to simulate the freeze–thaw environment. The project rocks are in a three-way stress state, and the freeze–thaw action triggers the water–ice phase change to produce the freeze expansion force, resulting in the derivation and expansion of internal fractures in the rock. Therefore, the lateral restraint is carried out by the fixture and the upper and lower ends of the fixture are sealed with gypsum mortar, so as to simulate the rock in a three-way force during the low-temperature freezing process, as shown in Figure 4. In addition, the effects caused by different freeze–thaw periods on the unloaded samples were mainly considered in the freeze–thaw environmental simulation tests. Therefore, a single freeze–thaw with a freezing temperature of −30 °C was chosen for the test, and three freezing periods were considered. They were frozen for 0 days, 7 days, and 14 days, and the specimens were thawed in a constant temperature water tank after the freezing was completed. Among them, the specimens frozen for 0 days were placed at room temperature.

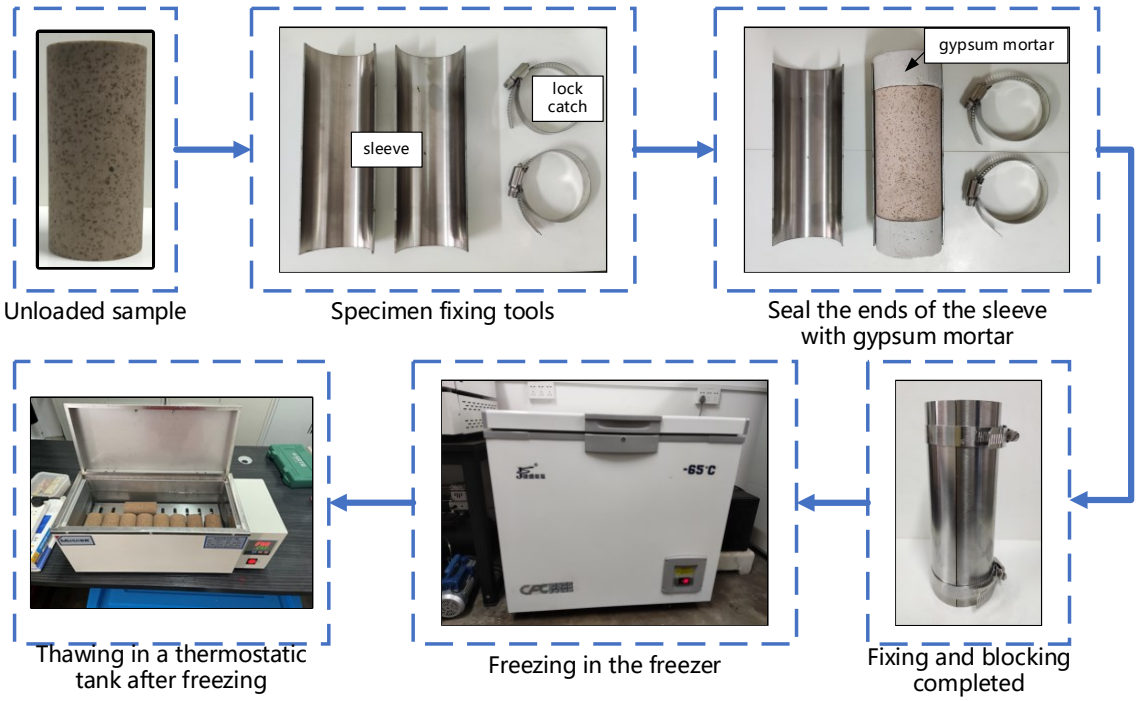

Figure 4. Freeze–thaw test procedure.

2.3. Triaxial Creep Test

Triaxial loading creep tests were carried out using the unloaded sandstone samples that completed the freeze–thaw simulation tests in Section 2.2. The creep test confining pressure value is the residual confining pressure value in the unloading test corresponding to the initial confining pressure condition. The creep test uses a graded loading stress path, and the loading levels were taken as 20%, 30%, 40%, 50%, 60%, and 70% of the triaxial peak strength of its corresponding initial confining pressure. There are various criteria regarding the duration of each load level; Yang [24] pointed out that, when the deformation increment is less than 0.003 mm every 24 h, the deformation is considered to reach stability and the next level of load can be applied. Tsai [25] used the stability boundary method to calculate that the specimen could reach creep stability within 24 h from the initial creep data. Gasc-Barbier [5] took 3 years to complete the creep test. The first method was adopted in this paper, while it was observed during the test that all levels of loading except for the damage phase could reach deformation stability within 12 h, so the loading time of 12 h was set uniformly for the convenience of subsequent comparisons, and the test groups are shown in Table 1.

Table 1. Experimental grouping.

Specimen Number	Initial Confining Pressure /MPa	Creep Confining Pressure /MPa	Freeze Period /Day
R15-0	15	6.75	0
R15-7			7
R15-14			14
R21-0	21	12	0
R21-7			7
R21-14			14

3. Results and Discussion

3.1. Loading Creep Curve of Unloaded Specimen

The loading creep curve mainly reflects the rock strain development process with the passing of time and the increase in stress level. Figure 5 shows the loading creep curves of unloaded samples under different conditions. In Figure 5, it can be seen that the overall trends of the creep test curves of the two groups with different values of confining pressure are the same, with the increase in stress level corresponding to the gradual changes in the creep stage: deceleration creep, stable creep, and accelerated creep are the three typical creep stages. Under the initial confining pressure of 15 MPa, the creep behaviour of specimen R15-0 of the normal temperature test group is not obvious, and the creep curve reflects that the strain of the specimen before the stress reaches the long-term strength is mainly the transient strain generated when the load is applied. The creep deformation accounts for a very small amount, and there is no obvious change in the axial and lateral directions of the specimen under the same creep time at different stress levels. Sample R15-7 is similar to sample R15-0 in terms of their creep curves at 7 days of freezing, and the creep deformation is not obvious before in the damage stage. In contrast, sample R15-14 is significantly different at 14 days of freezing, and the lateral expansion phenomenon is obvious at the 60% stress level. The lateral creep curve develops with a certain slope at this stage, and the strain also increases significantly. The creep curves of the three samples under the initial confining pressure of 21 MPa are significantly different. The creep damage of specimen R21-0 of the normal temperature test group occurs at a load level of 70%: the damage occurs suddenly and the creep curve is smooth before the damage stage. Test group R21-7 underwent damage during loading at the 70% load level, exhibiting significant lateral deformation before damage. For test group R21-14, at a load level of 60% after 1.5 h of creep damage, the creep curve exhibits a significantly accelerated creep phase. Comparing the initial confining pressures of the 15 MPa and 21 MPa test groups, the deformation of specimens with an initial confining pressure of 21 MPa is greater than that of specimens with an initial confining pressure of 15 MPa in the same freezing period before specimen damage occurs.

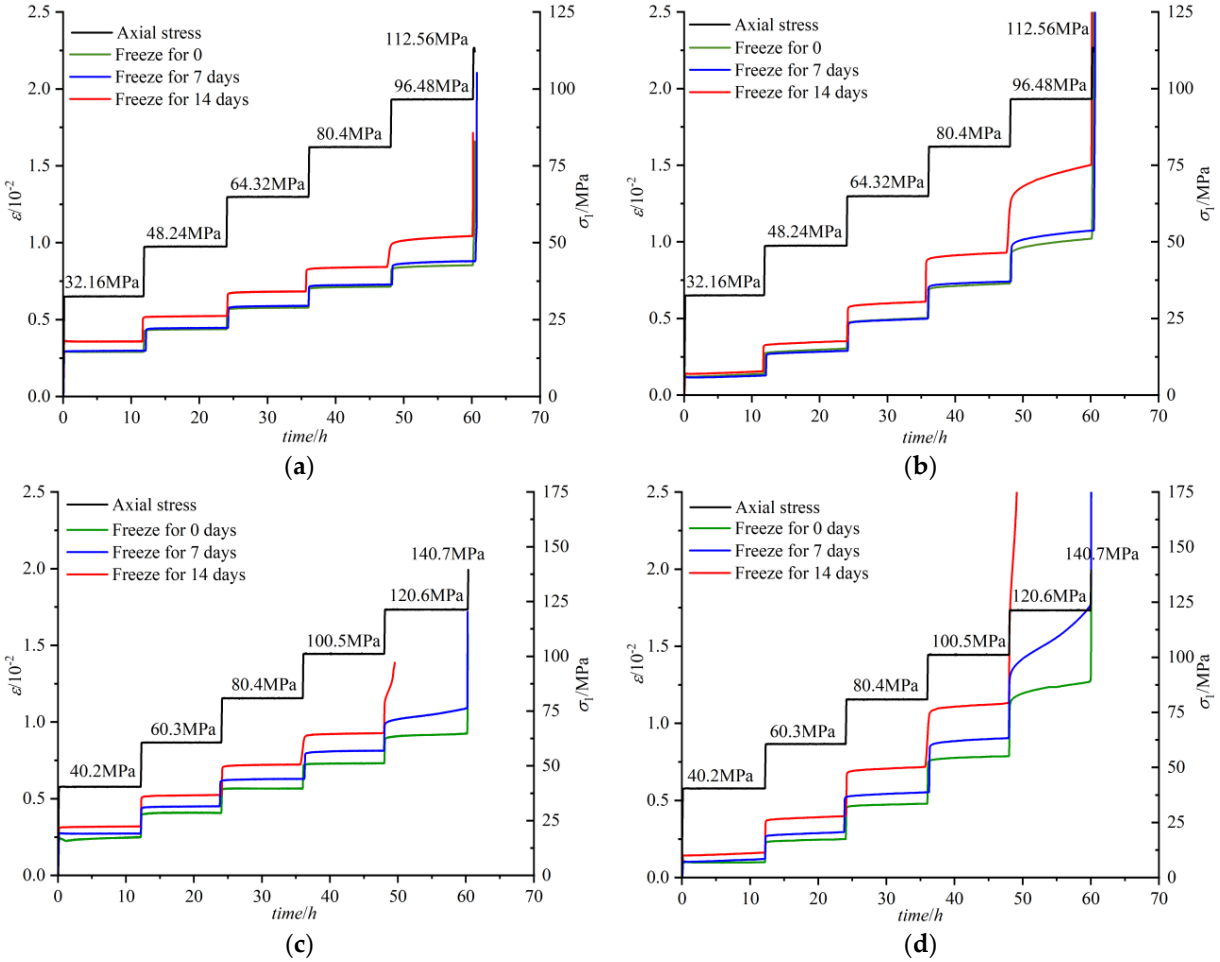

Figure 5. Loading creep curves for different confining pressure and different freezing periods (here, R15-0, R15-7, and R15-14 and R21-0, R21-7, and R21-14 are used to denote rock samples frozen for 0, 7, and 14 days under two types of confining pressure conditions, respectively. and (**a**) initial confining pressure 15 MPa, axial strain curve. (**b**) initial confining pressure 15 MPa, lateral strain curve. (**c**) Initial confining pressure 21 MPa axial strain curve. (**d**) initial confining pressure 21 MPa, lateral strain curve.)

Summarizing the above trends, firstly, the effect of freeze–thaw time on the deterioration of rock samples is not obvious when the initial confining pressure is relatively low. The reasons for this are that the relatively low initial confining pressure characterizes the relatively low unloading level and the structural damage caused by unloading is small; however, the degree of damage to the rock by a single freeze–thawing action depends on the number and size of cracks within the rock, and then the relatively low initial confining pressure corresponds to a smaller structural damage to the rock, resulting in weaker freeze–thaw deterioration. This also reflects that the unloading process is the main cause of structural damage in rock compared with freeze–thaw action, which is the main factor affecting the safety and stability of rock works. Secondly, the lateral creep behavior of the rock sample is more obvious than the axial when the initial confining pressure is the same. It is analyzed that, during the lateral unloading process, vertical cracks are easily generated in the specimen along the unloading direction, and the freeze swelling force generated by the water–ice phase change during the freeze–thaw action further increases the number and size of vertical cracks, leading to the obvious lateral expansion of the specimen in the subsequent creep test. Therefore, lateral support and monitoring of the rock in the excavation unloading area should be considered during the construction process, especially when the site is affected by a low temperature climate.

3.2. Strain Variation Characteristics

To further analyze the creep deformation characteristics of the unloaded sample at each stage, the creep data for each load level of the test group with an initial confining pressure of 15 MPa are summarized in Table 2. As shown in Table 2, the creep results of this test group show that the transient strain is the dominant contributor to the total strain, with R15-0, R15-7, and R15-14 transient strains accounting for 86%, 84%, and 78%, respectively. The strain development trends in the three groups of tests have consistent characteristics. For the transient strain, the axial transient strain in the process of increasing the stress level shows a general trend of decreasing and then increasing. At a low stress level, the deformation of the unloaded sample is mainly based on the transient elastic deformation occurring during loading. The increase in external load causes relative flow between sandstone particles, and the internal microscopic pores of the unloaded specimen are gradually compacted and deformed. This part of the deformation is closely related to the pore structure. As the load level increases, the internal pore volume of the unloaded sample shrinks, the deformation space gradually decreases, and the axial transient strain decreases. This happens until the stress level increases to a certain critical value, exceeding the load-bearing capacity limit of the rock structure, and damage occurs at some weak surfaces, at which time the plastic strain increases rapidly. The lateral transient strain is manifested as a lateral transient dilation with the application of axial stress, which increases steadily and significantly with the increase in stress. For creep strain, both the axial and lateral strains in the three sets of test results show a gradual increase with the increasing stress level, and the difference between them also increases. For sample R15-0, the axial creep strain is 39 με (1 με = 10^{-6}) and the lateral creep strain is 208 με at the first stress loading stage, with a difference of 169 με. As the stress continues to increase, the axial creep strain reaches 313 με and the lateral creep strain reaches 1217 με at the stage before damage, with a difference of 904 με. The magnitude of creep strain reflects the damage accumulation process of the unloaded sample, and the creep strain continues to increase as the load level increases and the damage of the unloaded sample intensifies.

Table 2. Creep strain for an initial confining pressure of 15 MPa.

Sample Number	σ_1 /MPa	Instantaneous Strain/10^{-3}		Creep Strain/10^{-3}	
		Axial	Lateral	Axial	Lateral
R15-0	32.16	2.877	1.198	0.039	0.208
	48.24	1.301	1.268	0.173	0.362
	64.32	1.166	1.491	0.223	0.510
	80.40	1.193	1.778	0.244	0.514
	96.48	1.006	1.657	0.313	1.217
	112.5	1.397	3.846	—	—
R15-7	32.16	2.840	1.119	0.143	0.159
	48.24	1.366	1.318	0.106	0.298
	64.32	1.253	1.689	0.178	0.401
	80.40	1.212	1.912	0.162	0.518
	96.48	1.187	2.049	0.357	1.273
	112.5	1.409	4.210	—	—
R15-14	32.16	3.493	1.351	0.091	0.235
	48.24	1.421	1.477	0.229	0.445
	64.32	1.356	1.996	0.242	0.5910
	80.40	1.293	2.350	0.304	0.844
	96.48	1.292	2.749	0.696	2.984
	112.5	1.388	4.764	—	—

The axial strain is larger than the lateral strain at the beginning of the stress loading, but, with the gradual increase in the stress level in the test process, the lateral strain gradually approaches and exceeds the axial strain, and the lateral expansion effect is significant, which is significantly different from the trend obtained from the conventional loading creep test (the axial strain is larger than the lateral strain). The analysis concluded that, during the unloading damage test, the lateral unloading behaviour led to a reduction

in the lateral restraint, and the sample produced axially oriented tensile cracks under the action of bias stress loading, which led to the release of surface stress and the structural relaxation of the sample. Then, the lateral structural weakening of the sample triggered a significant expansion phenomenon in the reloading creep test, which led to the lateral strain becoming greater than the axial strain.

Comparing the results of the normal temperature test group to those of the freeze–thaw test group, it can be found that the freeze–thaw action intensifies the creep deformation characteristics of the unloaded sample and that the creep strain percentage increases continuously with the extension of the freezing period. For example, considering R15-0 and R15-14, the percentage of the transient strain decreased from 86% to 78% with the extension of the freezing period, and the difference in the axial and lateral creep strains was approximately 1.5~2 times those of the stresses at all levels.

3.3. Creep Damage Characteristics of Unloaded Sample

The damage pattern of the unloaded sample under the different confining pressures of the two groups is shown in Figure 6. The damage pattern is mainly characterized by shear damage, but there are also some other types of local damage patterns. The number of apparent cracks produced in the unfrozen–thawed unloaded samples at a creep confining pressure value of 6.75 MPa damage is greater than the number at a confining pressure of 12 MPa, and the rupture surface is mainly oblique across the sample axis at the higher confining pressure of 12 MPa. After the freeze–thaw action, the damage characteristics of the unloaded samples are mainly in the form of through shear damage and more fine cracks are produced. At a creep confining value of 6.75 MPa, the number of cracks in the unloaded samples increases as the freezing period grows and the degree of fragmentation increases. At a creep confining pressure value of 12 MPa, the inclination of the main rupture surface increases with increasing freezing periods and the number of new cracks increases.

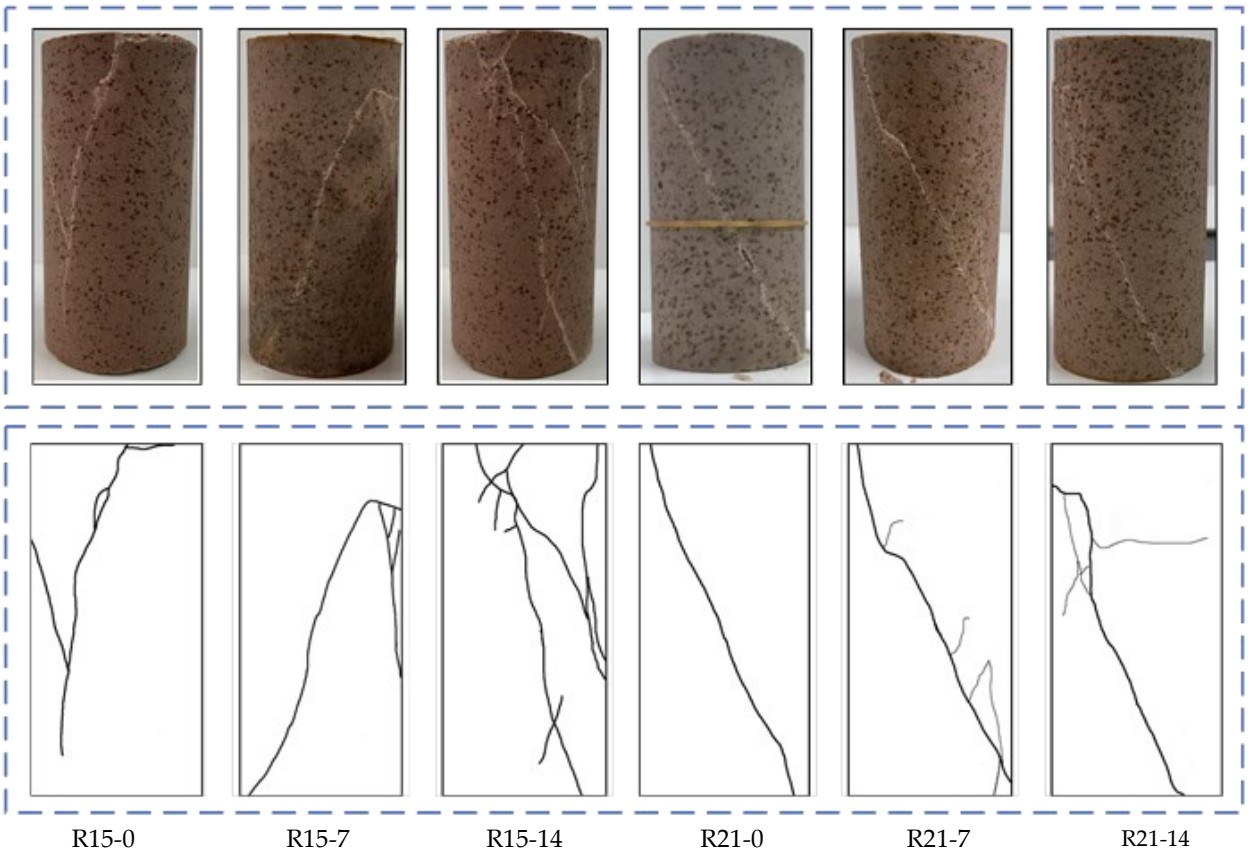

Figure 6. Creep damage characteristics of the unloaded sample under different conditions.

The analysis suggests that the freeze–thaw action intensifies the crack expansion and penetration of the unloading damage samples, as well as the new fracture derivation. The rupture surface spreading pattern of the unloaded damaged samples is mainly controlled by the confining pressure, and the freeze–thaw action further affects the rupture surface pattern. The water–ice phase change during the freeze–thaw process not only promotes the expansion of the main rupture surface, but also promotes the growth of secondary cracks when the unloaded samples are damaged.

3.4. Long−Term Strength Analysis of the Unloaded Sample

Long-term strength is an important safety indicator reflecting the stability of rock engineering. Under normal conditions, the long-term strength value of a rock is 60% to 90% of the instantaneous strength value. For unloaded rock, considering the excavation unloading effect, the stress state of the rock is changed. Additionally, its structural damage is intensified after freeze–thaw action, so it is very important to determine the long-term strength of this type of rock. Currently, the most widely used method for determining long-term strength is the isochronous curve cluster method. The isochronous curve cluster method is based on the Boltzmann superposition principle to superimpose the graded loading creep stress time curves and obtain the stress–strain isochronous curve cluster, with time as the parameter, and it is generally believed that the isochronous curve cluster will have a visible inflection point when the stress increases to a certain stage; the stress corresponding to this point is considered to be the long-term strength [26].

With the isochronous curve cluster method, isochronous curves were drawn. Figure 7 shows that the overall isochronous curve drawn at each time node consists of linear and nonlinear segments. At low stress levels, the rock deformation is mainly elastic deformation, which is reflected by the curves clustering together; with an increase in stress level, plastic deformation gradually dominates, which is reflected by the curve clustering changing from dense to loose. Using this method, the long-term strength of the unloaded sample under different conditions was determined, as shown in Table 3.

Table 3. Isochronous curve method to determine long-term strength under different conditions.

Sample Number	Long-Term Strength/MPa	Triaxial Peak StrengthMPa	Long-Term Strength/Triaxial Peak Strength
R15-0	87.52	160.8	54.4%
R15-7	85.53		53.2%
R15-14	83.22		51.7%
R21-0	110.14	201.0	54.7%
R21-7	106.64		53.0%
R21-14	90.12		44.8%

The above analysis shows that the long-term strength decay of unloaded samples at room temperature is mainly controlled by the unloading damage effect, and the long-term strength decay degree does not change significantly after the initial confining pressure increases, although the unloading confining pressure value increases. This also reflects the high confining pressure on the damage deterioration, and crack expansion of the unloaded sample has a suppressive effect. In addition, the slope excavation process is the main reason for the rapid release of stress and the deterioration of the rock structure. During the excavation and unloading process, the rock particle misalignment and fracture derivation provide a channel for the water body to intervene and provide conditions for the water–ice phase change caused by freezing and thawing. As shown in Table 3, the long-term strength decay of sandstone samples degraded by unloading damage superimposed on freeze–thaw periods has a certain correlation with the freezing time. Comparing the long-term strength results of unloaded sandstone samples under different freezing periods, it was found that the effect of freezing period on the long-term strength of unloaded samples of the same lithology has a certain threshold value.

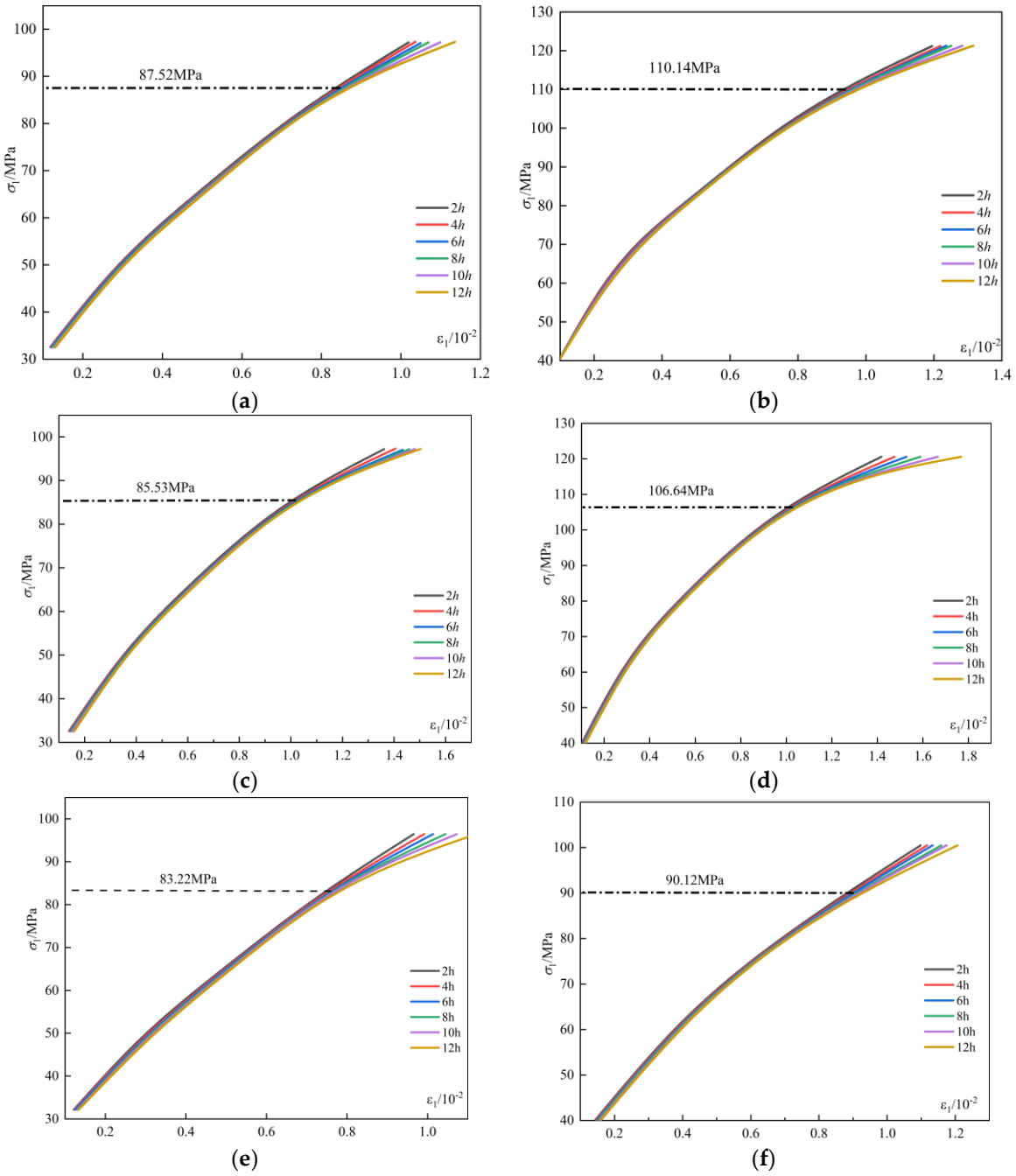

Figure 7. Isochronous curve cluster of the unloaded sample (where (**a**,**c**,**e**) and (**b**,**d**,**f**) are initial confining pressures of 15 MPa and 21 MPa, respectively). (**a**) R15-0. (**b**) R21-0. (**c**) R15-7. (**d**) R21-7. (**e**) R15-14. (**f**) R21-14.

4. Conclusions

In this paper, from the perspective of the complex environment of cold region reservoir bank slopes undergoing unloading disturbance and seasonal freeze–thaw erosion, we conducted triaxial unloading tests simulating the excavation disturbance process and seasonal freeze–thaw environment simulation tests. Finally, the loading creep test was carried out based on the division of the confining pressure value and freezing periods, and we compared and analyzed the deformation behavior, damage characteristics, and strength characteristics of sandstone samples subjected to unloading disturbance and freeze–thaw deterioration. Some conclusions are drawn as follows:

(1) During the unloading test, it was found that lateral expansion is the main form of unloading process. The degree of unloaded damage of rock samples is related to the stress level, the unloading response in the high stress state is more obvious, and the unloading process produces greater unrecoverable plastic damage. Therefore, the excavation and unloading process of rock in high ground stress areas should pay close attention to stress and lateral deformation monitoring to prevent the occurrence of engineering accidents such as rock bursts.

(2) During the graded loading creep test, it was found that the degradation effect of freeze–thaw on unloaded rock samples is controlled by the unloading level. The unloading process provides an action channel for the intervention of the water–ice phase change. Compared with freeze–thaw action, the unloading process is the main control factor causing the structural damage of the rock. In addition, the lateral strain of unloaded granite under freeze–thaw action is greater than the axial strain because of the nature of the unloading process and the mechanism of the freeze–thaw action.

(3) During the graded loading creep test, it was found that the creep strain was more significantly affected by the freeze–thaw action than the instantaneous strain, and it was related to the freezing period. Specifically, the creep rate under all levels of loading increases significantly when the freezing period increases.

(4) During the graded loading creep test, it was found that the creep damage pattern of the unloaded sample is mainly manifested as shear damage. Under a low confining pressure, the brittle characteristics of the unloaded sample are obvious, tensile cracks are produced in addition to the main rupture surface, and the number of cracks increases significantly after the freeze–thaw action. As the confining pressure increases, the plastic characteristics of the unloaded sample are enhanced, the rupture morphology is mainly an oblique shear rupture surface, and a small number of secondary cracks are produced along the rupture surface after the freeze–thaw action.

(5) During the graded loading creep test, it was found that the long-term strength of the unloaded sample is determined by the isochronous curve cluster method, and the calculation results show that the long-term strength of the sandstone decreases after the development of unloading damage and that the ratio of long-term strength to instantaneous strength is approximately 50~55%. The freeze–thaw action aggravates the structural damage of the unloaded sample, and the long-term strength of the unloaded sandstone gradually decreases and has a lower limit threshold with the extension of the freezing period.

(6) In fact, in addition to the freeze–thaw environment considered in this paper, there are also hydrological factors [27] (periodic wet and dry cycles in the slope of the reservoir bank excavation due to the rise and fall of the reservoir water), man-made hazards (fire in the tunnel triggers the strength decay of the unloaded rock), or man-made disturbances (cyclic loading due to the construction process) that can have a negative impact on the long-term mechanical properties of the excavated unloaded rock; this is also an influencing factor that will be considered in our subsequent study.

Author Contributions: Data curation, L.C. and S.G.; Investigation, L.C. and W.D.; Methodology, X.C., H.J., W.D. and S.G.; Writing—original draft, X.C. and H.J.; Writing—review and editing, X.C., H.J., L.C., W.D. and S.G. All authors have read and agreed to the published version of the manuscript.

Funding: This research was funded by The National Natural Science Foundation of China, grant number 51979218; The Joint Fouds of The National Natural Science Foundation of China, grant number U1965107; and The Natural Science Foundation of Shaanxi Province, grant number 2018JM5118. This support is gratefully acknowledged.

Institutional Review Board Statement: Not applicable.

Informed Consent Statement: Not applicable.

Data Availability Statement: All data, models, or code that support the findings of this study are available from the corresponding author upon reasonable request.

Conflicts of Interest: We declare that we have no known competing financial interests or personal relationships that could have appeared to influence the work reported in this paper.

References

1. Brantut, N.; Heap, M.J.; Baud, P.; Meredith, P.G. Mechanisms of time-dependent deformation in porous limestone. *J. Geophys. Res. Solid Earth* **2014**, *119*, 5444–5463. [CrossRef]
2. Sun, J. Rock rheological mechanics and its advance in engineering applications. *Chin. J. Rock Mech. Eng.* **2007**, *26*, 1081–1106. [CrossRef]
3. Benko, B.; Stead, D. The Frank slide: A reexamination of the failure mechanism. *Can. Geotech. J.* **1998**, *35*, 2. [CrossRef]
4. Suwa, H.; Mizuno, T.; Suzuki, S.; Yamamoto, Y.; Ito, K. Sequential processes in a landslide hazard at a slate quarry in Okayama, Japan. *Nat. Hazards* **2008**, *45*, 321–331. [CrossRef]
5. Gasc-Barbier, M.; Chanchole, S.; Bérest, P. Creep behavior of Bure clayey rock. *Appl. Clay Sci.* **2004**, *26*, 449–458. [CrossRef]
6. Mansouri, H.; Ajalloeian, R. Mechanical behavior of salt rock under uniaxial compression and creep tests. *Int. J. Rock Mech. Min. Sci.* **2018**, *110*, 19–27. [CrossRef]
7. Wang, C.L.; Zhou, B.K.; Li, C.F.; Cao, C.; Sui, Q.R.; Zhao, G.M.; Lu, H. Experimental investigation on the spatiotemporal-energy evolution pattern of limestone fracture using acoustic emission monitoring. *J. Appl. Geophys.* **2022**, *206*, 104787. [CrossRef]
8. Bodner, S.R.; Chan, K.S.; Fossum, A.F.; Munson, D.E. A Damage Mechanics Treatment of Creep Failure in Rock Salt. *Int. J. Damage Mech.* **1997**, *6*, 121–152. [CrossRef]
9. Damjanac, B.; Fairhurst, C. Evidence for a Long-Term Strength Threshold in Crystalline Rock. *Rock Mech. Rock Eng.* **2010**, *43*, 513–531. [CrossRef]
10. Innocente, J.C.; Paraskevopoulou, C.; Diederichs, M.S. Estimating the long-term strength and time-to-failure of brittle rocks from laboratory testing. *Int. J. Rock Mech. Min. Sci.* **2021**, *147*, 104900. [CrossRef]
11. Li, J.L. *The Theory and Application of Unloading Rock Mass Mechanics*; Architecture & Building Press: Beijing, China, 1999.
12. Chen, X.Z.; Chen, L.L.; Ma, B.; Zhang, X.; Du, W.; Wang, X.; Yang, C. Mechanical-characteristic evaluation of excavation unloading rock mass subject to high-temperature conditions. *Eng. Fail. Anal.* **2021**, *130*, 105757. [CrossRef]
13. Huang, X.; Liu, Q.S.; Kang, Y.S.; Pan, Y.C. Triaxial unloading creep experimental study of sandy mudstone. *Chin. J. Rock Mech. Eng.* **2016**, *35* (Suppl. S1), 2653–2662. [CrossRef]
14. Zhu, J.B.; Wang, B.; Wu, A.Q.; Hu, J.M. Study on rheological experiment and constitutive model of JINPING hydropower marble under unloading condition. Chin. *J. Solid Mech.* **2008**, *29* (Suppl. S1), 99–106. [CrossRef]
15. Tomanovic, Z. Rheological model of soft rock creep based on the tests on marl. *Mech. Time-Depend. Mater.* **2006**, *10*, 135–154. [CrossRef]
16. Chen, X.; Du, W.; Chen, L.; Ma, B.; Gong, S.; Jiang, H.; Wang, W. Mechanical Strength Decay Evaluation of Excavation Unloaded Rock Mass under Freeze-Thaw Conditions. *Appl. Sci.* **2022**, *12*, 12205. [CrossRef]
17. Hall, K. A laboratory simulation of rock breakdown due to freeze-thaw in a maritime Antarctic environment. *Earth Surf. Process. Landf.* **1988**, *13*, 369–382. [CrossRef]
18. Gasc-Barbier, M.; Merrien-Soukatchoff, V. Effect of Freezing-Thawing Cycles on the Elastic Waves' Properties of Rocks. *Geosciences* **2022**, *12*, 103. [CrossRef]
19. Deprez, M.; Kock, T.D.; Schutter, D.G.; Cnudde, V. A review on freeze-thaw action and weathering of rocks. *Earth-Sci. Rev.* **2020**, *203*, 1031043. [CrossRef]
20. Park, J.; Hyun, C.U.; Park, H.D. Changes in microstructure and physical properties of rocks caused by artificial freeze–thaw action. *Bull Eng. Geol. Environ.* **2014**, *74*, 555–565. [CrossRef]
21. Chen, G.Q.; Guo, F.; Wang, J.C.; Zhou, Y.X. Experimental study of creep properties of quartz sandstone after freezing-thawing cycles. *Rock Soil Mech.* **2017**, *38*, 203–210. [CrossRef]
22. Li, J.L.; Zhu, L.Y.; Zhou, K.P. Non-linear creep damage model of sandstone under freeze-thaw cycle. *J. Cent. South Univ.* **2021**, *28*, 954–967. [CrossRef]
23. *SL/T 264—2020*; Rock Test Procedure for Water Conservancy and Hydropower Engineering. China Water Power Press: Beijing, China, 2020.
24. Yang, S.Q. *Study on Rheological Mechanical Properties of Rock and Its Engineering Applications*; HoHai University: Nanjing, China, 2006.
25. Tsai, L.; Hsieh, Y.; Weng, M.; Huang, T.; Jeng, F. Time-dependent deformation behaviors of weak sandstones. *Int. J. Rock Mech. Min. Sci.* **2008**, *45*, 144–154. [CrossRef]
26. Schmidtke, R.H.; Lajtai, E.Z. The long-term strength of Lac du Bonnet granite. *Int. J. Rock Mech. Min. Sci. Geomech. Abs.* **1985**, *6*, 461–465. [CrossRef]
27. Lazar, M.; Aposu, I.; Faur, F.; Rotunjanu, I. Factors influencing the flooding process of former coal open-pits. *Min. Miner. Depos.* **2021**, *15*, 124–133. [CrossRef]